RSC Advances

ROYAL SOCIETY OF CHEMISTRY

www.rsc.org/advances

Extended dielectric constant step from -80°C to 336°C in the system $BaTiO_3$-$BiYO_3$-$Ba(Fe_{0.5}Nb_{0.5})O_3$

Yaru Wang, Yongping Pu*, Hanyu Zheng, Qian Jin, ziyan Gao

School of Materials Science & Engineering, Shaanxi University of Science and Technology, Xi'an 710021, China

Abstract

The polycrystalline $0.8BaTiO_3$-$(0.2-x)BiYO_3$-$xBa(Fe_{0.5}Nb_{0.5})O_3$ (0.8BT-(0.2-*x*)BY-*x*BFN) (*x*=0-0.04) ceramics are fabricated via a conventional solid state reaction method. The phase transition, microstructure and dielectric properties have been obtained by X-ray diffraction and dielectric measurements as a function of chemical composition and temperature. A progressive decline in ε_{rmax} with the elevation of *x* leads to near temperature-stable dielectric properties over a wide temperature range. For $x \geq 0$, dielectric measurements indicates relaxor behavior. The increasing amount of BFN content improves the dielectric temperature stability of BT ceramics effectively. For *x*=0.02, ε_r=590±15% from -48°C to 326°C and $tan\delta \leq 0.02$ across the temperature range -13-156°C. For *x*=0.04, ε_r=540±15% from -80°C to 336°C and $tan\delta \leq 0.02$ across the temperature range -22-231°C. The plot of the *ac* conductivity studies of *x*=0.04 shows the NTCR character of the compounds, and the activated energy of the dc conductivity is not far from the electron from second ionization of oxygen vacancies .

Key words: Dielectric temperature stability; Composites; *Ac* conductivity

1. Introduction

Increasing demand has triggered a stable growth both in the quantity in the variety of surface mount chip components, which in turn has led to continuing advances in integrated circuit packaging technology[1]. Multilayer ceramics capacitors (MLCC) are widely used in all kinds of

electronic products. Traditional high relative permittivity dielectrics based on barium titanate are specified to upper working temperatures of 125°C, 150°C, and 175°C for X7R, X8R, and X9R capacitors, respectively[2]. However, even X9R materials would not fulfill the requirements in some harsh conditions, such as oil drilling, aerospace and automotive environment[3]. For example, the anti-lock brake system sensors on wheels are required to work at the temperature range of 150-250°C, while in the cylinder the temperature is 200-300°C. Therefore, it is important that the field of materials work to broaden the working temperature to reach an ultra-broad temperature range (-55-300°C)[4]. This work has been sufficiently researched.

$BaTiO_3$ is a ferroelectric compound with the perovskite type structure and applies to capacitors due to its good dielectric properties. Doping or formatting solid solutions with other metal oxides or compounds is an effective approach to improve the properties of $BaTiO_3$ (BT). Among these additives, numerous solid solutions of BT with Bi-based perovskite compounds, such as $BaTiO_3$-$Bi(Zn_{0.5}Ti_{0.5})O_3$[5], $BaTiO_3$-$Bi(Mg_{0.5}Zr_{0.5})O_3$[6], $BaTiO_3$-$BiZn_{0.5}Ti_{0.5}O_3$-$BiScO_3$[7] have been reported. Recently, Wang et al. studied that the $Ba(Fe_{0.5}Nb_{0.5})O_3$ (BFN) ceramics generally exhibit a very high dielectric constant step over a broad temperature and frequency interval[8]. In our past studies, the relative permittivity as a function of temperature curves can be flatten gradually above the maximum permittivity with the $BiYO_3$ (BY). The distinctive properties of classical relaxor dielectrics are broad, frequency-dependent peaks in plots of relative permittivity versus temperature, and strong frequency dispersion in dielectric loss tangent[9-13].

In this study, BY and BFN are added to the BT ceramics in order to increase the dielectric properties. Furthermore, the effects of the addition of BY and BFN on the relaxor behavior, dielectric temperature stability have also been investigated.

2. Experimental Procedure

$0.8BaTiO_3$-(0.2-x)$BiYO_3$-xBa($Fe_{0.5}Nb_{0.5}$)O_3 (0.8BT-(0.2-x)BY-xBFN) (x=0-0.04) ceramics, were prepared via a conventional solid state reaction technique. The starting materials were high purity (99.9%) $BaCO_3$, TiO_2, Bi_2O_3, Fe_2O_3, Nb_2O_5, and Y_2O_3. The powders were dried in an oven at 200^{o}C for 24h and then weighed according to the stoichiometric ratios. All batches were mixed by ball-milling with zirconia grinding media in distilled water for 4h. After drying, the mixed powders were granulated with polyvinyl alcohol (PVA, 5wt%) and sieved through 80～40 mesh nylon sieve, then pressed into disks with 10mm in diameter and 1.5mm in thickness. The samples were heat treated at 600^{o}C for 30min to eliminate the PVA, then sintered at 1300^{o}C for 3h in air.

Phase structure of the ceramics was determined using X-ray diffraction (XRD D/max-2200PC, RIGAKU, Japan) patterns and Microstructures was studied by scanning electron microscope (JSM-6700, JEOL Ltd., Tokyo, Japan). To characterize the electrical properties, the specimens were ground polished to obtain parallel surfaces. In addition, silver paste was applied to opposite parallel faces and coated pellets were fired at 600^{o}C for 10min. The dielectric constant and loss were measured using a Hioki 3532-50, conduction behavior as a function of temperature (-100-200^{o}C) and frequency (20Hz-2MHz) were performed using an Agilent 4980A.

3.Results and discussion

3.1. X-ray diffraction study

Fig.1 shows the XRD patterns of BT and 0.8BT-(0.2-x)BY-xBFN (x=0-0.04) ceramics at optimized sintering temperatures. From Fig.1, there are no trace of secondary peak in all patterns with the detection limits of the instrument, suggesting that BFN and BY have diffused into the BT lattices to form a homogenous perovskite solid solution . It is clearly seen that the samples with pure BT and compositions of $x \leq 0.02$ display an obvious splitting of (002)/(200) diffraction peaks in accordance with the tetragonal symmetry (*P4mm* space group)[14]. The crystal structure transforms

to pseudocubic cubic symmetry when x=0.04. The (200) peaks shift continuously toward lower 2θ angles, indicating the increase of lattice parameters. Fig.2 reveals the microstructure of 0.8BT-(0.2-x)BY-xBFN (x=0.02, 0.04) ceramics at their optimized sintering temperatures. As seen in this figure, all samples are well sintered and exhibit a low porosity level.

Fig.3 shows the temperature dependence of relative permittivity (ε') and dielectric loss tangent ($tan\delta$) measured at various frequencies (1kHz, 10 kHz, 100 kHz, 1000 kHz) from room temperature to 400^{o}C. Composition BT exhibits a reasonably sharp Curie peak at ~120^{o}C. Frequency dispersion happens when x=0, the system transforms to a typical relaxor at x≥0. With the elevation of x, the relative permittivity of ceramics obviously decrease, and the permittivity-temperature plots exhibits near flat responses for composition x≥0. It is obvious that the BFN can increase the temperature stability of BT-based ceramics effectively. The maximum relative permittivity ε_{rmax} is ~7727 for x=0 at 1kHz, and then decreased to ~540 at x=0.04 which can be founded in Fig.3. With the increasing amount of BFN content, the typical change of the $T_{\varepsilon rmax}$ (the temperature of maximum permittivity) in 0.8BT-(0.2-x)BY-xBFN ceramics can be ascribed to the generation of Ti vacancies[15].

Temperature dependence of the reciprocal of relative permittivity for BT and 0.8BT-(0.2-x)BY-xBFN (x=0-0.04) ceramics at 1kHz is shown in Fig.4. ΔT_m , described by $\Delta T_m = T_{cw} - T_m$ (T_{cw} is the temperature at which ε starts to follow the Curie-Weiss law, and T_m is the temperature at which ε values reaches the maximum), is used to define the degree of deviation from Curie-Weiss law. ΔT_m elevates with x≥0, which suggests the increased dielectric diffuseness and enhanced relaxor behavior[16]. Deviation from the Curie-Weiss law is gradually clear in relaxor ferroelectrics with x≤0.04, as showed in Table 1.

Curie-Weiss analysis (Eq.(1))[19] confirmed typical ferroelectric behavior for BT and 0.8BT-(0.2-x)BY-xBFN (x=0-0.04) ceramics with a linear fit to plots of $1/\varepsilon$ versus T at $T>T_c$, and

T_c~T_o(Fig.4):

$$\varepsilon_r = \frac{C}{T-To} \quad (1)$$

Where C is the Curie-Weiss constant; T_o is the Curie-Weiss law.

The diffuse characteristics of ferroelectric-paraelectric phase transition are known to deviate from the typical Curie-Weiss behavior and can be described by a modified Curie-Weiss relationship[17-19]:

$$\frac{1}{\varepsilon_r} - \frac{1}{\varepsilon_m} = \frac{(T-T_m)^\gamma}{C} \quad (2)$$

Where ε_m is the maximum value of dielectric constant, ε is the dielectric constant at temperature T, T_m is the temperature at the peak of the dielectric constant, C is the Curie constant, and γ is the indicator of the degree of diffuseness, giving information on the character of the phase transition, γ is between 1 and 2, the values γ=1 and 2 are related to a normal ferroelectric and an ideal relaxor[20], respectively. Thus the value of γ can also be used to characterize the relaxor behavior.

The plot of ln($1/\varepsilon$-$1/\varepsilon_m$) as a function of ln(T-T_m) for BT and 0.8BT-(0.2-x)BY-xBFN (x=0-0.04) ceramics at 1kHz is shown in Fig.5 by fitting with Eq.(2) to calculate the γ value. The results are 1.72, 1.8, and 1.9 at 1kHz for x=0, x=0.02, and x=0.04, respectively, implying the strong relaxor behavior, The diffuse phase transition and deviation from Curie-Weiss type may be assumed due to disordering[21].

The diffuseness of the phase transition is described by an empirical parameter ΔT_{dif}, which is defined as $\Delta T_{dif1kHz} = T_{0.9\varepsilon m1kHz} - T_{\varepsilon m1kHz}$, where $T_{\varepsilon m1kHz}$ denotes the temperature of the dielectric maximum and $T_{0.9\varepsilon m1kHz}$ represents the higher temperature of 90% of the dielectric maximum at 1kHz. Yet another parameter, which is used to characterize the degree of relaxation behavior in frequency range of 1kHz-1000kHz, is described as $\Delta T_{relax} = T_{m1000kHz} - T_{m1kHz}$[22]. The values of ΔT_{dif} and ΔT_{relax} for BT and 0.8BT-(0.2-x)BY-xBFN (x=0-0.04) ceramics are shown in Table1. To

recapitulate, the above empirical characterization with the Curie-Weiss law (ΔT_m) and parameter (γ, ΔT_{dif} and ΔT_{relax}) represents that 0.8BT-(0.2-x)BY-xBFN are indeed a relaxor with diffuse phase transition and frequency dispersion.

One of the most desirable properties for MLCC materials is the temperature stability of dielectric permittivity. Fig.6 shows the temperature coefficients for 0.8BT-(0.2-x)BY-xBFN (x=0-0.04) ceramics at their maximum sintered densities. Increasing the BFN content to x=0.04 produces a broad relaxor dielectric peak. At x=0 the temperature variation in ε_r lay within ±15% of the value of 830 from -33^{o}C to 173^{o}C and $tan\delta$ values are ≤0.02 across the temperature range 27-276^{o}C. For x=0.02, ε_r=590±15% from -48^{o}C to 326^{o}C and $tan\delta$≤0.02 across the temperature range -13-156^{o}C. Furthermore, the temperature range of tanδ≤0.02 expands from -22-231^{o}C at x=0.04. While $\Delta\varepsilon/\Delta\varepsilon_{25}\leq\pm15\%$ in the temperature range of -80-336^{o}C for x=0.04, which indicates the more BFN addition can improve the thermal stability of BT ceramics.

Fig.7 shows the polarization-electric field response measured at room temperature. The BT exhibits typical ferroelectric hysteresis loop. With increasing x, the polarization-electric loops become narrow and have a low dielectric loss, which indicates the BFN content eliminate ferroelectric properties. These results would be in accordance with the XRD results, the paraelectric and cubic phase exist in the ceramics, so the polarization-electric plots are in the form of narrow ellipsoids with the elevation of x.

The plot of Z' versus Z'' (Nyquist or Cole-Cole plots) at different temperatures is shown in Fig.8. All the semicircles are depressed instead of a semicircle centered on the real axis, which indicates non-Debye type relaxation mechanism. Two semicircles can be observed in the two diagrams, which show that two distinct dielectric relaxation process exist in the samples, and the suppressed semicircular arcs indicate two different contributions from the grain interior and grain

boundary.

In order to obtain reliable values for resistance of grain and grain boundary and establish a connection between microstructure and electrical properties, the equivalent circuit model shown in Fig.8 is employed, which is based on the brick layer model[23]. In Fig.8, R_s is the resistance of lead used in the equipment, R_g is the resistance associated with grain, and *CPE* is a constant phase element indicating the departure from ideal Debye-type model. The *CPE* admittance is $Y_{CPE} = A_o(j\omega)^n = A\omega^n + jB\omega^n$, with

$$A = A_o \cos(\tfrac{n\pi}{2}), B = A_o \sin(\tfrac{n\pi}{2}) \quad (3)$$

Where A_o and n are parameters depending on temperature only, A_o confines the magnitude of the disperation.

According to Jonscher, the origin of the frequency dependence of conductivity is due to the relaxation of ionic atmosphere after the movement of the particle. The variation of *ac* conductivity as a function of frequency at different temperatures is shown in Fig.9. Jonscher make an attempt to explain the behavior of *ac* conductivity using the following universal power law[24]:

$$\sigma(\omega) = \sigma_0 + A\omega^n \quad (4)$$

Where $\sigma(\omega)$ is the total conductivity, σ_0 is the frequency independent or *dc* part, which is related to *dc* conductivity and the second term of constant phase element (*CPE*) type. The n ($0<n<1$) represents the degree of interaction between mobile ions with lattices around them, and A determines the strength of polarization[25].

It is reported that, the value of n can be larger than unity and there is no physical argument to restrict the value of n below 1[26]. In some glassy, mixed oxide and in single crystal reported value of n is greater than 1. We have fitted conductivity data using Eq.(9) with origin software suing non-linear curve fitting option and obtained the same of σ_0, A_0, n and are tabulated in Table 2. It can

be seen with decrease in temperature the value of *n* decreases.

Extrapolating these curves at low frequencies gives the *dc* conductivity (σ_{dc}). The resulting σ_{dc} is plotted as the function of reciprocal temperature in Fig.10 and it well obeys the Arrhenius relation:

$$\sigma = \sigma_0 \exp(-E_{cond} / K_B T) \quad (5)$$

where σ_0 is the pre-exponential term and E_{cond} is the conduction activation energy. The experimental values of conduction activation, E_{cond}=0.8eV, is near to 1eV which is the conduction activated energy of the electron from second ionization of oxygen vacancies[27]. Therefore, the conducting species in this temperature range is likely to come from the second ionization of oxygen vacancies $V_{\ddot{o}}$ as reported by Li at al[28].

4. Conclusions

Electrical properties of 0.8BT-(0.2-*x*)BY-*x*BFN (*x*=0-0.04) ceramics have been studied. X-ray powder diffraction patterns verifies that all samples exhibits a single phase perovskite structure and the transformation from tetragonal symmetry to pseudocubic occurs at 0.02≤*x*≤0.04. Compositions 0≤*x*≤0.04 are relaxor dielectircs. Stability in values of relative permittivity over a wide temperature range is demonstrated for *x*=0.04, with the temperature range of tanδ≤0.02 expands from -22-231^{o}C at *x*=0.04, and $\Delta\varepsilon/\Delta\varepsilon_{25}\leq\pm15\%$ in the temperature range of -80-336^{o}C. The polarization-electric plots are in the form of narrow ellipsoids with the elevation of *x*. Comparisions of dielectric properties with other materials proposed for high temperature capacitor applications indicates that such a material system could be suitable for high-temperature stable dielectric applications.

Acknowledgments

This research was supported by the National Natural Science Foundation of China (51372144) and the Key Program of Innovative Research Team of Shaanxi Province (2014KCT-06).

References

[1] S.F. Wang, J.H. Li, Y.F. Hau, Y.C. Wu, Y.C. Lai, M.H. Chen, J. Eur. Ceram. Soc., 2013, 33, 1793-1799.

[2] A. Zeb, S. J. Milne, J. Am. Ceram. Soc., 2013, 96, 3701-3703.

[3] J.B. Lim, S. Zhang, N. Kim, T.R. Shrout, J. Am. Ceram. Soc., 2009, 92, 679-682.

[4] L.X. Li, J.X. Chen, D. Guo, N. Zhang, M.J. Wang, Y.R. Liu, Ceram. Int., 2014, 40, 12539-12543.

[5] Raengthon N, Cannn DP, J. Am. Ceram. Soc., 2011, 95, 1064-1612.

[6] A. Zeb, S. J. Milne, J. Eur. Ceram. Soc., 2014, 34, 3159-3166.

[7] Raengthon N, Sebastian T, Cumming D, Reaney IM, Cann DP, J. Am. Ceram. Soc., 2012, 95, 3554-3561.

[8] Z. Wang, M.R. FANG, H.J. Li, Y.F. Wen, C. Wang, Y.P. Pu, Compos. Sci. Technol., 2015, 117, 410-416.

[9] Bokov AA, Ye Z-G, J. Mater. Sci., 2006, 41, 31-52.

[10] HC Wang, Schulze WA, J. Am. Ceram. Soc., 1990, 73, 825-832.

[11] V.V. Shvartsman, D.C. Lupascu, J. Am. Ceram. Soc., 2012, 95, 1-26.

[12] Laulhé C, Hippert F, Kreisel J, Maglione M, Simon A, Hazemann JL, V. Nassif, Phys. Rev. B., 2006, 74, 014106-1–12.

[13] Badapanda T, Rout SK, Cavalcante LS, Sczancoski JC, Panigrahi S, Longo E, M Siu Li, J. Phys. D. Appl. Phys., 2009, 42, 175414-1–9.

[14] X.L. Chen, J. Chen, D.D. Ma, L. Fang, H.F. Zhou, Ceram. Int., 2015, 41, 2081-2088.

[15] Wang SF, Li JH, Hsu YF, Wu YC, Lai YC, Chen MH, J. Eur. Ceram. Soc., 2013, 33, 1793-1799.

[16] Ravez J, Simon A, J. Solid. State. Chem., 2001, 162, 260-265.

[17] Morrison FD, Sinclain DC, West AR, J. Appl. Phys., 1999, 86, 6355-6366.

[18] Raengthon N, Cannn DP, J. Am. Ceram. Soc., 2011, 95, 1064-1612.

[19] Zhu F, Skidmore T. A, Bell, A. J, Comyn T. P, James C.W, Ward M, et al, Mater. Chem. Phys., 2011, 129, 411-417.

[20] Zhang Q, Li Z, Li F, Xu Z, J. Am. Ceram. Soc., 2011, 94, 4335-4339.

[21] S. Mahajanl, O. P. Thakur, J. Phys. D. Appl. Phys., 2009, 42, 065413.

[22] D Liu,Y.P. Pu, J.L. Li, X Shi, Ceram. Int., 2013, 39, 593-596.

[23] Q.Q. Ke, X.J. Lou, J Wang, Phys. Rev. B., 2010, 82, 024102.

[24] M.A.L. Nobre, S. Lanfredi, J. Appl. Phys., 2003, 93, 5576.

[25] M. Vijayakumar, S. Selvasekarapandian, M. S. Bhuvaneswari, G. Hirankumar, G. Ramprasad, R. Subramanian, P.C. Angelo, Physica. B., 2003, 334, 390-397.

[26] D.K. Pradhan, B. Behera, P.R. Das, J. Mater. Sci-Mater El., 2012, 23,779-785.

[27] Z. Wang, X. M. Chen, L. Ni, Y.Y. Liu, X.Q. Liu, Appl. Phys. Lett., 2007, 90, 102905.

[28] G. B. Li, S. X. Liu, F. H. Liao, S. J. Tian, X. P. Jing, J. H. Lin, Y. Uesu, K. Kohn, K. Saitoh, M. Terauchi, N. L. Di, Z. H. Cheng, J. Solid. State. Chem., 2004, 177, 1695-1703.

Table Captions

Table 1 T_m、 T_c、 T_{cw}、ΔT_m、ε_m、γ、ΔT_{dif} and ΔT_{relax} for BT and 0.8BT-(0.2-*x*)BY-*x*BFN (*x*=0-0.04).

Table 2 *Ac* Conductivity Parameters.

Table 1 T_m、 T_c、 T_{cw}、ΔT_m、ε_m、γ、ΔT_{dif} and ΔT_{relax} for BT and 0.8BT-(0.2-x)BY-xBFN (x=0-0.04).

	T_m	T_c	T_d	ΔT_m	γ	ΔT_{dif}	ΔT_{relax}
BT	118.85	112.58	121.79	2.94	1.01	2.00	2.54
x=0	70.62	106.82	168.99	98.37	1.72	49.08	19.94
x=0.02	68.04	83.06	175.86	107.82	1.80	60.12	29.9
x=0.04	56.21	110.32	196.79	140.58	1.90	61.2	30.2

Table 2. *Ac* Conductivity Parameters.

Temperature	σ_0	A	n
400°C	1.03099E-4	2.84424E-8	0.66679
375°C	5.53743E-5	1.64396E-8	0.69812
350°C	3.0749E-5	1.2738E-8	0.70998
325°C	1.58963E-5	1.09789E-8	0.71346
300°C	7.18377E-6	7.63512E-9	0.73059

Figure captions

Fig.1. X-ray diffraction pattern of BT and 0.8BT-(0.2-x)BY-xBFN (x=0-0.04) ceramics.

Fig.2. SEM micrographs of (a) x=0.02, (b) x=0.04.

Fig.3. Temperature dependent relative permittivity (ε') and loss tangent ($tan\delta$) for compositions (a) BT, (b) x=0, (c) x=0.02, (d) x=0.04.

Fig.4. Temperature dependence of the reciprocal of relative permittivity ($1/\varepsilon$) for (a) BT, (b) x=0, (c) x=0.02, (d) x=0.04. The symbol represents experimental data points, and the solid straight black line show the fitting to the Curie-Weiss law.

Fig.5.Values of $\ln(1/\varepsilon - 1/\varepsilon_m)$ as a function of $\ln(T-T_m)$ for (a) BT, (b) x=0, (c) x=0.02, (d) x=0.04. The symbol represents experimental data points, symbols represent the data and solid lines the degree of fit.

Fig.6. Temperature coefficient of ε for 0.8BT-(0.2-x)BY-xBFN (x=0-0.04) ceramics: ε_{25} is the dielectric permittivity at 25^{o}C.

Fig.7. Polarization-electric field, P-E, loops for (a) BT ceramics, (b) 0.8BT-(0.2-x)BY-xBFN (x=0-0.04) ceramics.

Fig.8. Nyquist plots of Z' and Z'' 0.8BT-0.16BY-0.04BFN ceramics at different temperature (inset of equivalents circuit model used here in associated with brick layer model).

Fig.9. Frequency dependence of *ac* conductivity at different temperatures of 0.8BT-0.16BY-0.04BFN ceramics.

Fig.10. Temperature dependence of conductivity for 0.8BT-0.16BY-0.04BFN ceramics.

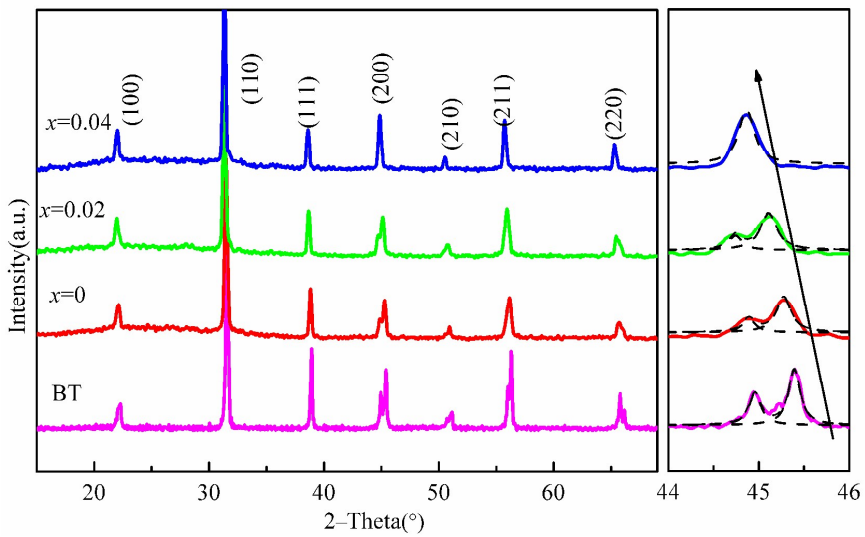

Fig.1. X-ray diffraction pattern of BT and 0.8BT-(0.2-*x*)BY-*x*BFN (*x*=0-0.04) ceramics.

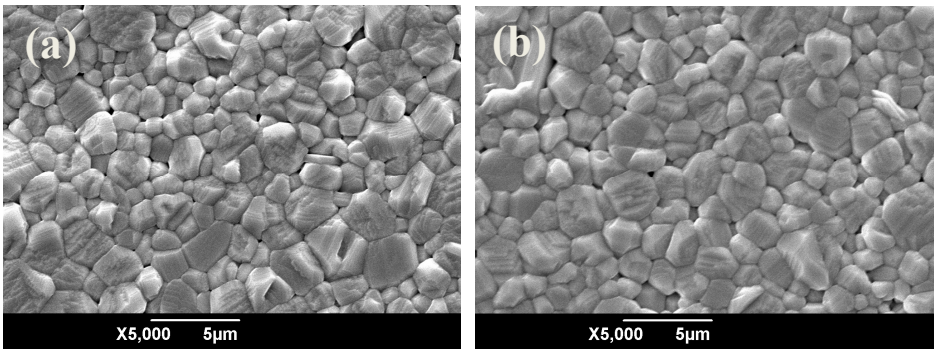

Fig.2. SEM micrographs of (a) x=0.02, (b) x=0.04.

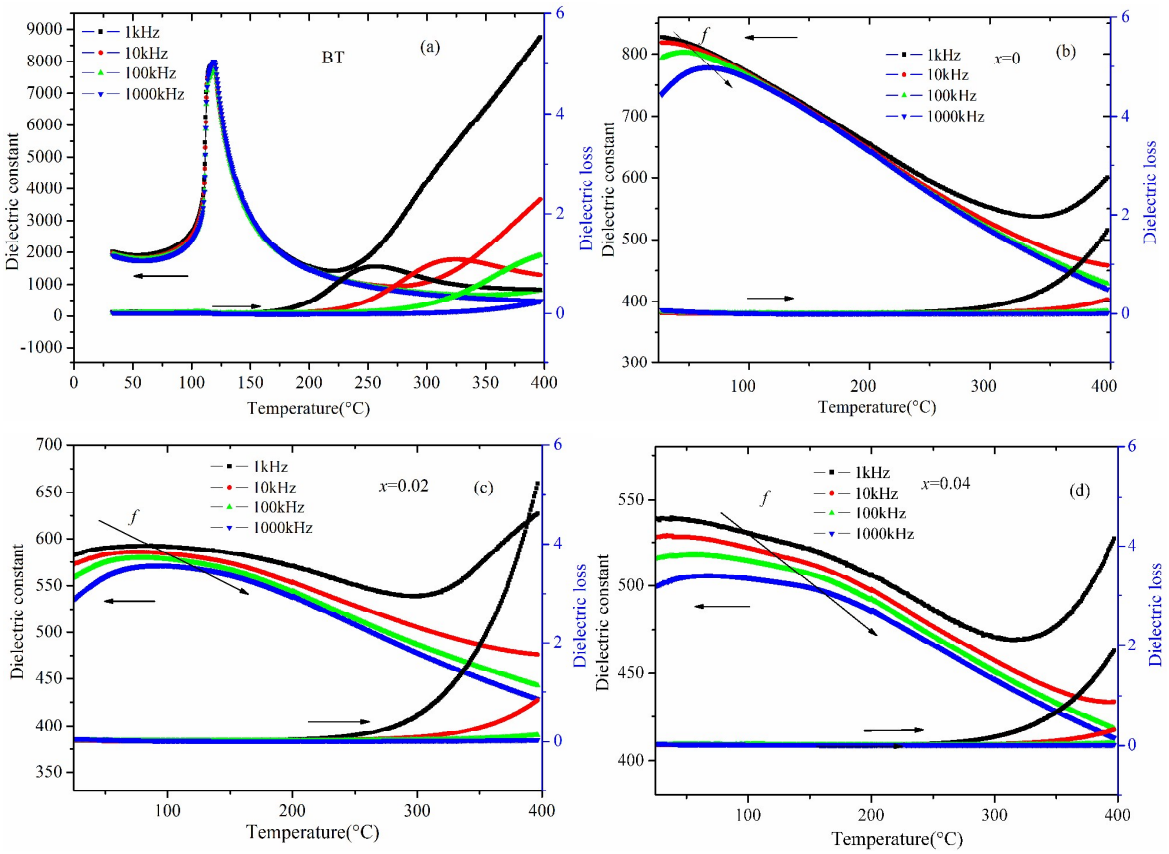

Fig.3. Temperature dependent relative permittivity (ε') and loss tangent ($tan\delta$) for compositions (a) BT, (b) x=0, (c) x=0.02, (d) x=0.04.

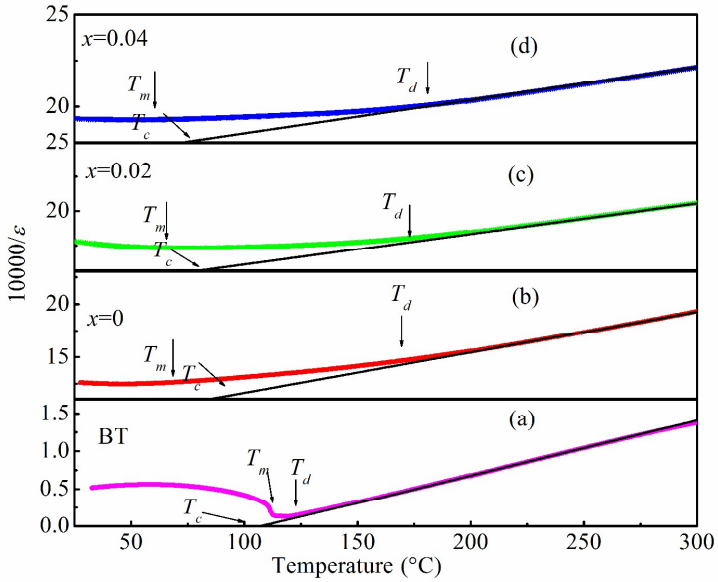

Fig.4. Temperature dependence of the reciprocal of relative permittivity ($1/\varepsilon$) for (a) BT, (b) x=0, (c) x=0.02, (d) x=0.04. The symbol represents experimental data points, and the solid straight black line show the fitting to the Curie-Weiss law.

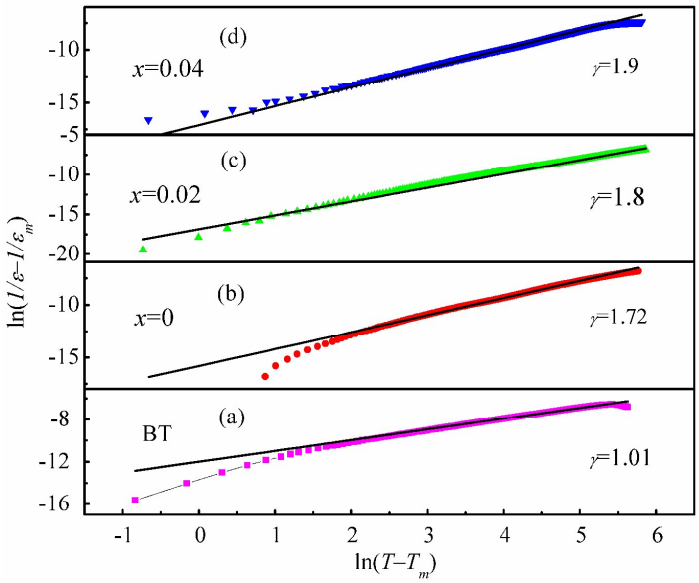

Fig.5. Values of $\ln(1/\varepsilon-1/\varepsilon_m)$ as a function of $\ln(T-T_m)$ for (a) BT, (b) x=0, (c) x=0.02, (d) x=0.04. The symbol represents experimental data points, symbols represent the data and solid lines the degree of fit.

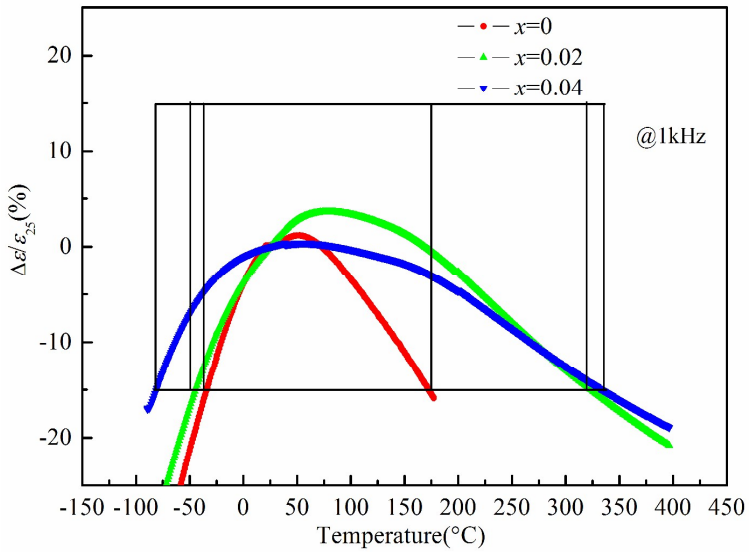

Fig.6. Temperature coefficient of ε for 0.8BT-(0.2-x)BY-xBFN (x=0-0.04) ceramics: ε_{25} is the dielectric permittivity at 25^{o}C.

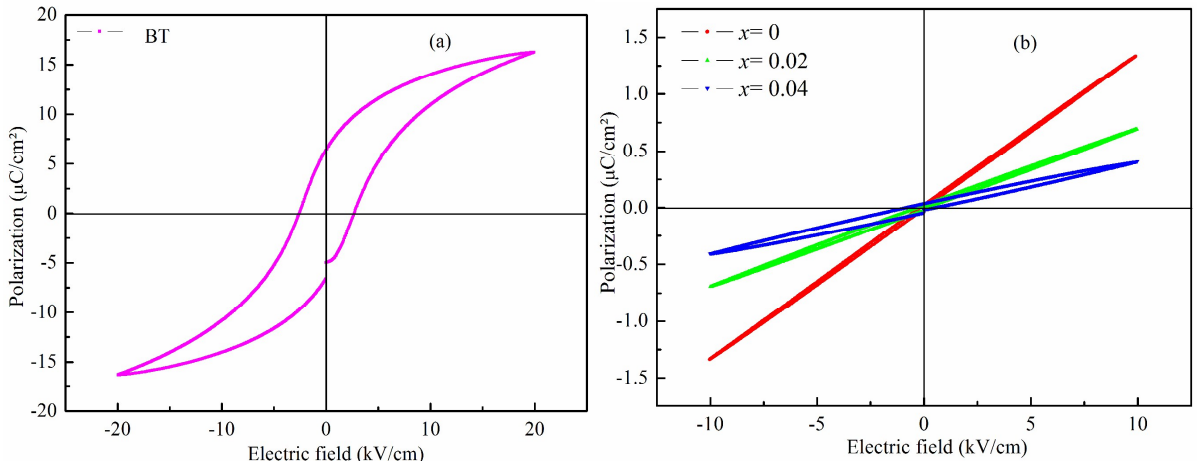

Fig.7. Polarization-electric field, *P*-*E*, loops for (a) BT ceramics, (b) 0.8BT-(0.2-*x*)BY-*x*BFN (*x*=0-0.04) ceramics.

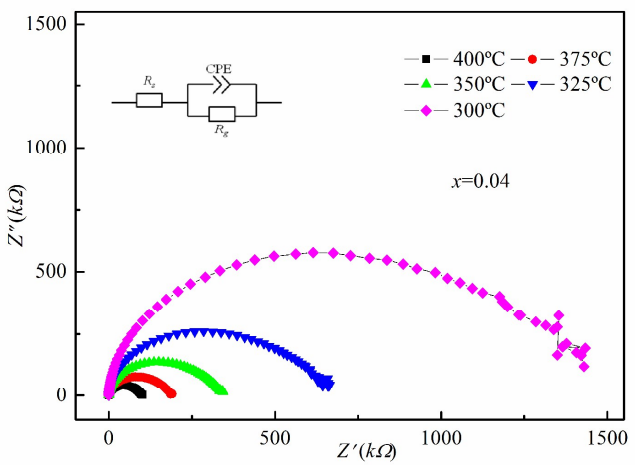

Fig.8. Nyquist plots of Z' and Z'' 0.8BT-0.16BY-0.04BFN ceramics at different temperature (inset of equivalents circuit model used here in associated with brick layer model).

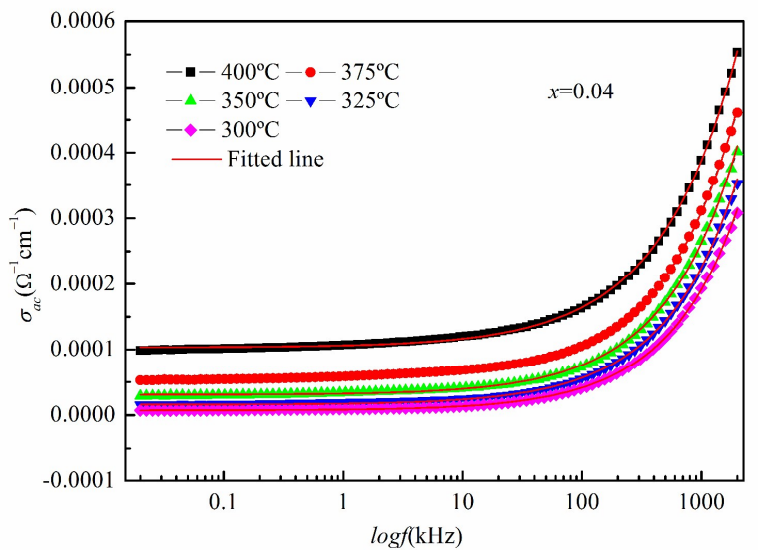

Fig.9. Frequency dependence of *ac* conductivity at different temperatures of 0.8BT-0.16BY-0.04BFN ceramics.

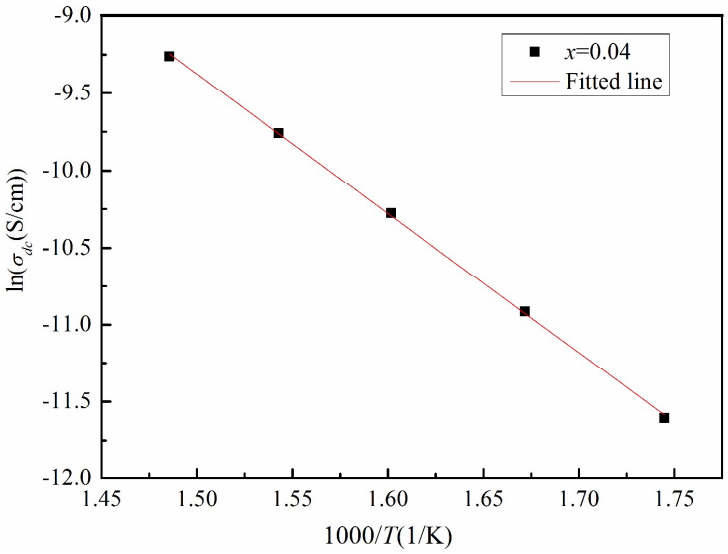

Fig.10. Temperature dependence of conductivity for 0.8BT-0.16BY-0.04BFN ceramics.